



Enhanced Motion Planning for Differential Drive Mobile Robots Using C^1 -Continuous Double Clothoid Segments

Mohd Fazril Izhar Mohd Idris¹ , Ahmad Ramli² , Wan Zafira Ezza Wan Zakaria³ 

¹Universiti Sains Malaysia and Universiti Teknologi MARA, Perlis Branch, fazrilizhar@uitm.edu.my

²Universiti Sains Malaysia, alaramli@usm.my

³Universiti Sains Malaysia, ezzafira@usm.my

Corresponding author: Ahmad Ramli, alaramli@usm.my

Abstract. This article introduces a novel method to improve motion planning for differential drive robots, with a focus on the Pioneer 3-DX model. By applying principles from Computer-Aided Geometric Design (CAGD), specifically clothoid curves, the study presents a double clothoid segments that integrates standard and mirrored clothoids. This approach offers enhanced flexibility in determining tangent directions, thereby simplifying trajectory design. Additionally, ensuring C^1 continuity guarantees smooth transitions in tangent directions between the clothoid segments, enhancing the overall smoothness of the generated trajectories. Through rigorous formulation and numerical methods, the study demonstrates the effectiveness of double clothoid segments in generating smooth trajectories. Incorporating this approach into the motion planning of the Pioneer 3-DX robot, validated through simulation, exhibits consistent and versatile performance, suggesting its potential to transform robotic motion planning across various applications.

Keywords: motion planning, differential drive, mobile robot, clothoid segments.

DOI: <https://doi.org/10.14733/cadaps.2025.1086-1104>

1 INTRODUCTION

The realm of robotics has experienced a profound evolution, propelled by advancements in technology and a growing demand for robots capable of navigating complex and dynamic environments [22]. Whether it be in industrial automation, service robotics, or autonomous vehicles, the ability to plan and execute motion with precision is essential for the effectiveness and safety of robotic systems [9],[18]. At the heart of this capability lies motion planning, a fundamental process through which robots determine optimal trajectories to navigate from an initial state to a desired goal while avoiding collisions with obstacles [27],[30].

Among the diverse array of robotic platforms, differential drive mobile robots stand out for their simplicity, maneuverability, and versatility. These robots, characterized by two independently driven wheels, are

commonly employed in various applications, including exploration, surveillance, and logistics [20]. However, achieving efficient and smooth motion with such robots, especially in cluttered or unknown environments, poses significant challenges that necessitate sophisticated motion planning strategies [32].

Motion planning for differential drive robots involves navigating a high-dimensional state space to determine trajectories that minimize a specified cost function while adhering to various constraints, such as obstacle avoidance and the robot's kinematic limitations [14]. The non-holonomic nature of differential drive robots complicates the planning process, as they lack the ability to move sideways and must rely on precise steering actions to maneuver in confined spaces [21]. Conventional motion planning algorithms like potential fields and rapidly exploring random trees (RRT) often face challenges in generating smooth and efficient trajectories for differential drive robots, particularly in environments with narrow passages or complex geometries [6].

Efficiently managing time and energy is vital for optimizing robot movements to minimize both duration and energy consumption in reaching their destinations. [10] introduced the Neural Field for Optimal Motion Planner (NFOMP) algorithm to tackle optimal motion planning in cluttered environments, producing smooth trajectories faster than sampling-based and discrete algorithms, albeit with a relatively high computational demand. Similarly, [19] applied the Generalized Regression Neural Network (GRNN) technique to enhance navigation path lengths and reduce errors for differential drive robots compared to feedforward neural networks. However, this approach constrained robot movements to straight lines, resulting in intermittent halts during directional changes. [23] focused on energy optimization for differential drive wheeled mobile robots using a Genetic Algorithm Fuzzy Logic Controller (GA-FLC). While effective in reducing energy consumption, this method relied on knowing predetermined routes like zigzag, square, sharp turn, straight, diamond-shaped, circular, and figure-eight paths, rather than autonomously generating such paths.

To address these challenges, recent research has explored alternative approaches to motion planning, emphasizing principles from Computer-Aided Geometric Design (CAGD). Clothoid curves, characterized by smoothly varying curvature profiles, have emerged as a promising tool for trajectory generation in robotics [12]. Offering advantages over traditional polynomial-based trajectory planning methods, clothoids feature continuous curvature profiles and smooth transitions between segments, leading to more natural and efficient robot motion [28].

The clothoid curve, also known as the Cornu Spiral or Euler Spiral, is extensively utilized across various disciplines, including road design, railway engineering, and robotics, owing to its distinctive geometric properties [3]. The standard parametric formulation of the clothoid curve was established by [25], which incorporates the Fresnel integral as the foundation for deriving the clothoid equation. Additionally, the generalization of the clothoid can be observed in the Aesthetic curve when $\alpha = -1$, which utilizes logarithmic functions as its basis in the formula [31]. Although both being capable of producing the same clothoid curve, these formulations stem from vastly different equations.

Despite the potential benefits of clothoid curves, integrating them into motion planning algorithms poses several challenges. Previous research has highlighted issues such as computational complexity, parameterization, and the need for effective path smoothing techniques to ensure feasibility and optimality of generated trajectories [11]. Furthermore, while clothoid-based approaches have shown promise in specific applications, their scalability and adaptability to diverse robotic platforms and environments remain areas of ongoing investigation [2].

Research by [8] utilized clothoid curves to generate paths for real Two-Wheel-Drive Autonomous Mobile Robots, encountering challenges in reaching target points despite the real robot's paths closely resembling those of several points that combined line segments and clothoid curves in their experiments. Similar issues arose in Nguyen's study [24], where experiments with Differential-Drive Mobile Robots (DDMR) faced problems with position and posture errors of their real robots due to considerations of wheel slip and road surface conditions. These scenarios warrant further investigation in the future, as currently, simulations offer limited relief in obtaining better research outcomes.

Simulation holds significant advantages for robotics research, offering a cost-effective, safe, and scalable

platform for experimentation and analysis. Unlike physical experiments, simulations require minimal resources and pose no risk to personnel or equipment, making them particularly advantageous for exploring complex or hazardous scenarios. Additionally, simulations provide researchers with precise control over experimental conditions, enabling systematic testing and evaluation of algorithms under various circumstances.

Moreover, simulations facilitate rapid prototyping and iteration, allowing researchers to quickly modify parameters and assess their impact on robot behavior. With realistic modeling capabilities for robot dynamics, sensors, and environments, simulations offer a valuable tool for advancing robotics technologies and understanding robot performance in diverse scenarios.

In this article, we present an innovative double clothoid approach designed to enhance motion planning for differential drive mobile robots. The simulation of the robot trajectory using double clothoid segments has been conducted utilizing the CoppeliaSim simulator, a widely used robotics simulation platform. To evaluate the performance of the proposed approach, we compare the generated paths with existing studies [27], providing analysis of trajectory smoothness, efficiency, and flexibility.

While this study closely aligns with the approach of combining two clothoids as seen in [15] and [26], there are differences in the method used to generate mirrored segments. In [26], a technique known as the control polyline was employed to guide composite curves during the design phase. This involved creating clothoid splines by pairing clothoids as blending curves, where pairs could be symmetric or unsymmetric. In cases of symmetry, one clothoid's starting point (where curvature is zero) was positioned on an adjacent edge meeting the bisector, with its tangent vector perpendicular to the bisector. The second clothoid was then determined by reflecting the first about the bisector. In contrast, our study utilized a straight line $x=y$ for this reflection. Additionally, researchers were afforded the flexibility to determine the tangent direction at both the starting and ending points of the planned movement, distinguishing it from previous methodologies.

The planning section of this paper begins with an introduction in Sec. 1, providing an overview of the motivation and objectives of the study. We then delve into the specifics of differential drive mobile robots, highlighting their unique characteristics and challenges in motion planning which can be found in Sec. 2. Next, we detail the methodology used to implement double clothoid segments for trajectory generation, including the formulation of the trajectory generation algorithm and the simulation setup described in Sec. 3. Subsequently, in Sec. 4 we present the results of our experiments, analyzing the effectiveness of the proposed approach and comparing it with existing methods. Finally, we discuss the implications of our findings, potential avenues for future research, and conclude with closing remarks on the significance of the study in Sec. 5.

2 MOBILE ROBOT

The Pioneer 3-DX robot, made by Adept MobileRobots, is known for its versatility and reliability. With two independently driven wheels, it can move in any direction with precision, making it useful for tasks like navigation, surveillance, and research [1].

Its sturdy design suits a variety of purposes in research, education, and industry. Using its differential drive system, it can navigate tight spaces and complex environments with ease. Equipped with sensors like laser range finders and cameras, it can perceive its surroundings accurately. Its modular design allows for easy integration of additional sensors and equipment, making it adaptable to different tasks. Fig. 1 depicts the simulated Pioneer 3-DX robot from CoppeliaSim simulator.

However, it's noteworthy that this study implements a sensorless mode, foregoing the use of sensors typically found in the Pioneer 3-DX robot. Despite the absence of sensors, the robot's differential drive system still enables precise movements in various environments.

Differential drive robots, with their unique steering mechanism, can move with agility. By adjusting the speeds of their wheels independently, they can execute various movements efficiently. This simplicity makes them cost-effective and suitable for educational and research purposes.

In motion planning, these robots face challenges due to their steering constraints. Advanced planning

algorithms are needed to generate smooth trajectories. Innovations like double clothoid segments offer ways to improve motion planning, ensuring smoother trajectories for robots like the Pioneer 3-DX.



Figure 1: Pioneer 3-DX Simulated Robot

3 METHODOLOGY

The clothoid curve, alternatively referred to as the Cornu Spiral or Euler Spiral, is a mathematical construct characterized by a consistent rate of curvature [7]. Renowned for its unique geometric properties, this curve finds extensive applications in diverse fields such as road design, railway engineering, and robotics [13],[16],[5]. Its intrinsic ability to provide seamless transitions between curves of varying radii renders it indispensable in motion planning scenarios where gradual changes in curvature are imperative.

3.1 Clothoid Formulation

The standard clothoid formulation [25], denoted as $C_s(t, \theta, i) = [X_s(t, \theta, i), Y_s(t, \theta, i)]$ is delineated by the following parametric equations:

$$X_s(t, \theta, i) = x_i + a_i [\cos(\theta) c(t) - \sin(\theta) s(t)], \quad (1)$$

$$Y_s(t, \theta, i) = y_i + a_i [\sin(\theta) c(t) + \cos(\theta) s(t)], \quad (2)$$

where $t \in R, 0 \leq \theta \leq \frac{\pi}{2}$ and i represent the i^{th} curve. Here, (x_i, y_i) denotes the initial point for the clothoid curve, while a_i signifies the scaling factor determined by the product of π, R_i and A_i with R_i representing the curve's radius and A_i is a positive parameter. The Fresnel integrals, $c(t)$ and $s(t)$ are integral components of clothoid formulation, defined as:

$$c(t) = \int_0^t \cos\left(\frac{\pi u^2}{2}\right) du. \quad (3)$$

$$s(t) = \int_0^t \sin\left(\frac{\pi u^2}{2}\right) du. \quad (4)$$

Conversely, the mirrored clothoid formulation, denoted as $C_m(t, \theta, i) = [X_m(t, \theta, i), Y_m(t, \theta, i)]$, represents a reflection of the standard clothoid across the x-axis, coupled with a rotation dependent on θ within the range of 0 to $\frac{\pi}{2}$, yielding:

$$X_m(t, \theta, i) = x_i + a_i [\cos(\theta) c(t) - \sin(\theta) s(t)], \quad (5)$$

$$Y_m(t, \theta, i) = y_i + a_i [-\sin(\theta) c(t) - \cos(\theta) s(t)], \quad (6)$$

where, (x_i, y_i) denotes the initial point for the mirrored clothoid curve, while a_i signifies the scaling factor determined by the product of π, R_i and A_i . A mirrored clothoid can be visualized as the reflection of the standard clothoid across the line $y = x$, achieved by setting the rotation angle to $\frac{\pi}{2} - \theta$, where θ represents

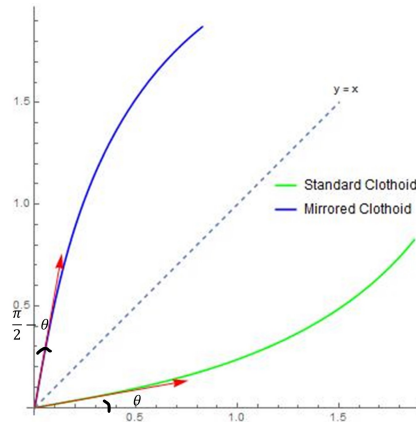


Figure 2: Standard and mirrored clothoids.

the angle of the standard clothoid from the x-axis. This alternative representation simplifies the determination of mirrored clothoids. The incorporation of mirrored clothoids enables the development of double clothoid segments, wherein they can be combined with other clothoids. Fig. 2 provides a visual representation of standard and mirrored clothoids.

3.2 Double Clothoid Segments

Our novel clothoid approach encompasses four distinct categories, each offering unique characteristics and applications: both standard clothoids, both mirrored clothoids, mirrored-standard clothoids and standard-mirrored clothoids.

These categories are visually represented in Fig. 3, showcasing the distinct characteristics and applications of each configuration. Through our novel clothoid approach, we aim to offer engineers and designers a comprehensive toolkit for trajectory planning and motion control, catering to diverse requirements and preferences in various domains.

We would like to highlight that, in most cases depicted in Fig. 3c, 3d, and others akin to Fig. 4a, 4d, and Fig. 5a, 5c, a single clothoid segment suffices for resolution, as evidenced by [31]. Nonetheless, in instances like those in Fig. 3a, 3b and 6b, employing the double clothoid segment method is pivotal to fortifying the robustness of this study.

The actual scenario unfolds when all four categories of double clothoid segments are generated from the values of θ_1 , representing the initiation of movement direction, and θ_2 , representing the termination of movement direction, suitable for obtaining solutions that connect between two clothoids, namely standard and mirrored. Not all θ values can be taken to obtain these category results. We will demonstrate more specific calculations based on this statement later.

The procedure for generating these double clothoids is based on equation from (1) to (6). The second clothoid segment, D_2 is derived from the first segment, D_1 through a sequence of transformations, including rotation, translation and reflection. Both D_1 and D_2 can be represented as either standard clothoids, C_s or mirrored clothoids, C_m . Specifically, D_1 that connected to (x_1, y_1) can be expressed as follows: $D_1(t, \theta, 1) = [X_s(t, \theta, 1), Y_s(t, \theta, 1)]$ or $[X_m(t, \theta, 1), Y_m(t, \theta, 1)]$ while D_2 that connected to (x_2, y_2) can be written as follows: $D_2(t, \theta, 2) = [X_s(t, \theta + \pi, 2), Y_s(t, \theta + \pi, 2)]$ or $[X_m(t, \theta + \pi, 2), Y_m(t, \theta + \pi, 2)]$.

To optimize the combinations of these clothoids, we employ a rigorous approach based on two fundamental

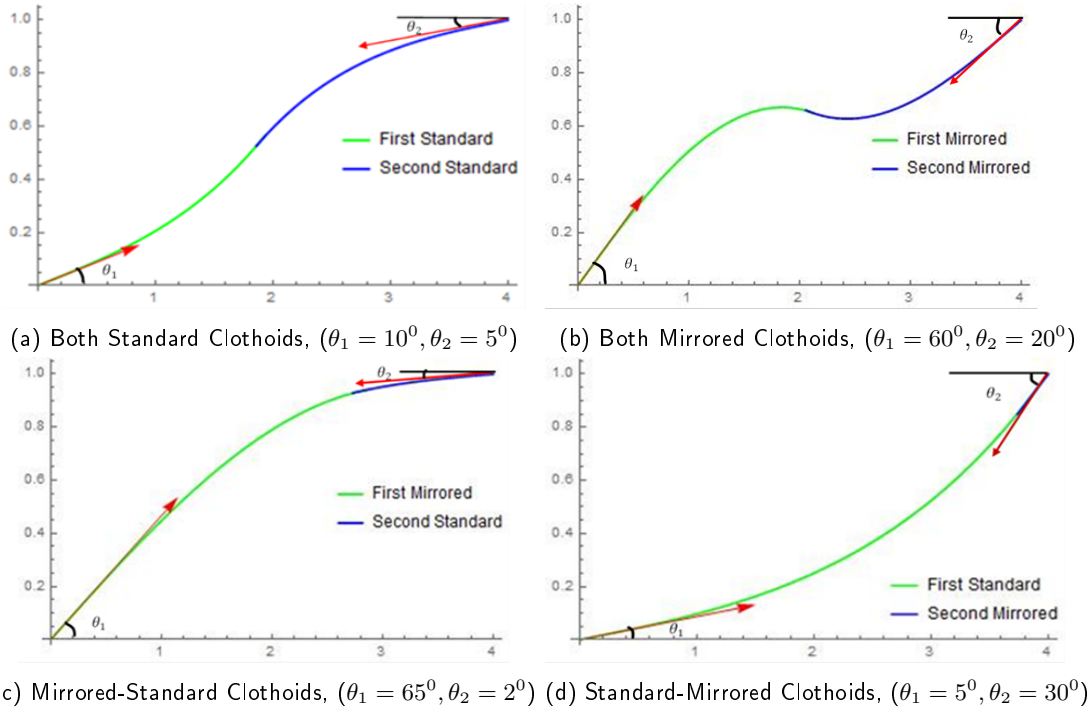


Figure 3: Illustration of four variations of double clothoid segments, showcasing specific examples of tangent angles, θ at the starting and ending points.

conditions:

$$D_1(A_1, \theta_1, 1) = D_2(A_2, \theta_2, 2). \quad (7)$$

$$D'_1(A_1, \theta_1, 1) = -D'_2(A_2, \theta_2, 2). \quad (8)$$

Equation (7) marks the initial condition, underscoring the necessity of upholding C^0 continuity to seamlessly link clothoid segments. C^0 continuity ensures that the curve's position remains uninterrupted, devoid of sudden shifts or discontinuities. Put simply, a curve that adheres to C^0 continuity appears smooth and uninterrupted, lacking any visible breaks. Moving forward, Equation (8), the second condition enforces C^1 continuity, which mandates a smooth transition in tangent directions between these segments. These criteria play a pivotal role in determining four crucial parameters: the radii of curvature for the initial and subsequent clothoids, R_1 and R_2 , along with the parameters A_1 and A_2 . Notably, all parameters must remain greater than zero to uphold the validity and continuity of the clothoid curves.

In our study, we preserve C^1 continuity for motion planning as seen in Equation (8), ensuring smooth direction changes at junction points, ideal for basic point-to-point navigation. While G^2 continuity promises even smoother transitions in curvature rates, making trajectories exceptionally seamless, we opted for C^1 for its simplicity and effectiveness. C^1 continuity maintains consistent tangent directions along the curve, ensuring smooth transitions between segments. On the other hand, G^2 continuity takes it a step further by ensuring both continuous tangent directions and curvature rates, perfect for smoother paths.

We acknowledge that using only C^1 continuity results in jumps in curvature. However, the trajectories and robot simulations have still met our desired targets. Additionally, the calculations involved in achieving G^2 continuity are more complex, requiring careful adjustment and matching of parameters. This process

is sensitive to numerical precision and computation, and demands sophisticated optimization algorithms to minimize differences in curvature at the joining points, which can be computationally expensive and complex. [4] also highlights that obtaining a solution is not always guaranteed and often requires a more intricate process. However, for our study's purposes, C^1 continuity proved sufficient, offering a straightforward solution to our navigation needs. Nonetheless, we envision implementing a G^2 continuous path in our future studies.

Here we present a more specific process on how to obtain solutions for double clothoid segments. We consider an example to obtain solutions for the 'standard-mirrored clothoid' category. Let D_1 be the standard clothoid segment, C_s , and D_2 be the mirrored clothoid segment, C_m .

From Equations (1), (2), (5), (6), and (7), we can derive the following equations:

$$x_1 + \pi R_1 A_1 [\cos(\theta_1) c(A_1) - \sin(\theta_1) s(A_1)] = x_2 + \pi R_2 A_2 [\cos(\theta_2 + \pi) c(A_2) - \sin(\theta_2 + \pi) s(A_2)] \quad (9)$$

$$y_1 + \pi R_1 A_1 [\sin(\theta_1) c(A_1) - \cos(\theta_1) s(A_1)] = y_2 + \pi R_2 A_2 [-\sin(\theta_2 + \pi) c(A_2) - \cos(\theta_2 + \pi) s(A_2)] \quad (10)$$

Furthermore, from Equation (8), we can deduce the following equation.

$$\begin{aligned} & \pi R_1 A_1 \left[\cos(\theta_1) \cos\left(\frac{\pi A_1^2}{2}\right) - \sin(\theta_1) \sin\left(\frac{\pi A_1^2}{2}\right) \right] \\ & = \pi R_2 A_2 \left[-\cos(\theta_2 + \pi) \cos\left(\frac{\pi A_2^2}{2}\right) + \sin(\theta_2 + \pi) \sin\left(\frac{\pi A_2^2}{2}\right) \right] \end{aligned} \quad (11)$$

$$\begin{aligned} & \pi R_1 A_1 \left[\cos(\theta_1) \cos\left(\frac{\pi A_1^2}{2}\right) + \sin(\theta_1) \sin\left(\frac{\pi A_1^2}{2}\right) \right] \\ & = \pi R_2 A_2 \left[\cos(\theta_2 + \pi) \cos\left(\frac{\pi A_2^2}{2}\right) + \sin(\theta_2 + \pi) \sin\left(\frac{\pi A_2^2}{2}\right) \right] \end{aligned} \quad (12)$$

We employ four equations, namely Equation (9) to (12), to find solutions for four parameters: A_1 , A_2 , R_1 , and R_2 , while also establishing the values of θ_1 and θ_2 beforehand. To effectively solve for these parameters, various numerical methods can be employed. One efficient approach is through the utilization of built-in functions in software packages such as Mathematica. The built-in function "FindRoot" in Mathematica employs the bisection method to locate solutions to the equation of 'zero-finding'. In this context, the solution for the equation is consistently precise due to the constraint that the entering clothoid must precisely intersect the initial position. These tools offer computational capabilities that expedite the parameter-solving process, facilitating rapid and accurate determination of the clothoid parameters.

It is essential to emphasize that in other categories, such as 'both standard', our focus is solely on ensuring that both segments D_1 and D_2 adhere to the C_s formula, while in 'both mirrored', both segments utilize C_m . Conversely, in the 'mirrored-standard' category, D_1 corresponds to C_m , and D_2 corresponds to C_s .

3.3 Double Clothoid on Differential Drive Mobile Robot

We leveraged this state-of-the-art path generation technique to craft motion plans tailored for differential drive mobile robots, with a specific emphasis on the Pioneer 3-DX model. Our methodology involved deploying the robot's motion simulations through the CoppeliaSim simulator platform, seamlessly integrated with the Matlab remote API. This integration empowered us to precisely emulate and assess the robot's behavior across diverse scenarios, facilitating extensive testing and fine-tuning of our motion planning algorithms. This study adopted the same approach as detailed in [27] for robot kinematics and simulation. Additionally, the simulations are conducted on a high-capacity computer equipped with an Intel Core i5 12th Generation, 12400 2.5GHz Processor, 16GB DDR4 RAM, and a 1TB SSD drive. This robust hardware configuration ensures efficient simulation execution, enabling the exploration of complex scenarios and large datasets.

4 RESULT AND DISCUSSION

In this section, we illustrate the process of selecting viable and appropriate categories based on the chosen tangent angles for the beginning and end of the trajectory. Subsequently, we present the simulation results of robot movements based on all four categories of double clothoid segments. Finally, we compare these results with previous study based on categories suitable for the trajectories created in this study.

4.1 Selection of Double Clothoid Segment Categories

This study is able for users to flexibly determine the tangent direction for robot trajectory movements at the starting and ending points. However, at present, it still requires a manual process to determine the appropriate category to be selected based on these chosen angles. In this study, we experimented with the starting point (0,0) and the ending point (4,1) across various tangent angles. The suitability of double clothoid segment categories was determined based on the obtained solutions when both clothoids were connected. If no solutions were obtained, they were not selected. However, if there is more than one solution where both clothoids are connected at the same tangent angle, the selection is made based on the condition of the minimum arc length.

For the purpose of discussion, we conducted three examples named Case I, II and III of variations in the tangent angle values of θ_1 and θ_2 . These cases were run for each category to obtain their respective solutions. Here, it is shown that some categories have solutions while others do not. The process to obtain parameter values using the methods stated in the preceding section is demonstrated.

4.1.1 Case I: $\theta_1 = 3^0$, $\theta_2 = 30^0$

For the 'standard-mirrored clothoid' category, we utilized Equations (9) to (12), resulting in the following equations:

$$\begin{aligned} 0 + \pi R_1 A_1 \left[\cos\left(\frac{3\pi}{180}\right) c(A_1) - \sin\left(\frac{3\pi}{180}\right) s(A_1) \right] \\ = 4 + \pi R_2 A_2 \left[\cos\left(\frac{30\pi}{180} + \pi\right) c(A_2) - \sin\left(\frac{30\pi}{180} + \pi\right) s(A_2) \right] \end{aligned} \quad (13)$$

$$\begin{aligned} 0 + \pi R_1 A_1 \left[\sin\left(\frac{3\pi}{180}\right) c(A_1) - \cos\left(\frac{3\pi}{180}\right) s(A_1) \right] \\ = 1 + \pi R_2 A_2 \left[-\sin\left(\frac{30\pi}{180} + \pi\right) c(A_2) - \cos\left(\frac{30\pi}{180} + \pi\right) s(A_2) \right] \end{aligned} \quad (14)$$

$$\begin{aligned} \pi R_1 A_1 \left[\cos\left(\frac{3\pi}{180}\right) \cos\left(\frac{\pi A_1^2}{2}\right) - \sin\left(\frac{3\pi}{180}\right) \sin\left(\frac{\pi A_1^2}{2}\right) \right] \\ = \pi R_2 A_2 \left[-\cos\left(\frac{30\pi}{180} + \pi\right) \cos\left(\frac{\pi A_2^2}{2}\right) + \sin\left(\frac{30\pi}{180} + \pi\right) \sin\left(\frac{\pi A_2^2}{2}\right) \right] \end{aligned} \quad (15)$$

$$\begin{aligned} \pi R_1 A_1 \left[\cos\left(\frac{3\pi}{180}\right) \sin\left(\frac{\pi A_1^2}{2}\right) + \sin\left(\frac{3\pi}{180}\right) \cos\left(\frac{\pi A_1^2}{2}\right) \right] \\ = \pi R_2 A_2 \left[\cos\left(\frac{30\pi}{180} + \pi\right) \sin\left(\frac{\pi A_2^2}{2}\right) + \sin\left(\frac{30\pi}{180} + \pi\right) \cos\left(\frac{\pi A_2^2}{2}\right) \right] \end{aligned} \quad (16)$$

These four equations, (13) to (16) were simultaneously solved to obtain the parameter values of A_1 , A_2 , R_1 , and R_2 , using the built-in function "FindRoot" in Mathematica, yielding the solution values of $A_1 = 0.5423$, $A_2 = 0.0768$, $R_1 = 3.9629$, and $R_2 = 27.9815$. The existence of these values indicates that this category

can be chosen as double clothoids. These values were then used to generate the plotted graph as shown in Fig. 4d.

For the 'both standard' category, we manipulated Equations (9) to (12) to adjust the involved formulas, resulting in the following equations:

$$\begin{aligned}
 &0 + \pi R_1 A_1 \left[\cos\left(\frac{3\pi}{180}\right) c(A_1) - \sin\left(\frac{3\pi}{180}\right) s(A_1) \right] \\
 &= 4 + \pi R_2 A_2 \left[\cos\left(\frac{30\pi}{180} + \pi\right) c(A_2) - \sin\left(\frac{30\pi}{180} + \pi\right) s(A_2) \right]
 \end{aligned} \tag{17}$$

$$\begin{aligned}
 &0 + \pi R_1 A_1 \left[\sin\left(\frac{3\pi}{180}\right) c(A_1) - \cos\left(\frac{3\pi}{180}\right) s(A_1) \right] \\
 &= 1 + \pi R_2 A_2 \left[\sin\left(\frac{30\pi}{180} + \pi\right) c(A_2) - \cos\left(\frac{30\pi}{180} + \pi\right) s(A_2) \right]
 \end{aligned} \tag{18}$$

$$\begin{aligned}
 &\pi R_1 A_1 \left[\cos\left(\frac{3\pi}{180}\right) \cos\left(\frac{\pi A_1^2}{2}\right) - \sin\left(\frac{3\pi}{180}\right) \sin\left(\frac{\pi A_1^2}{2}\right) \right] \\
 &= \pi R_2 A_2 \left[-\cos\left(\frac{30\pi}{180} + \pi\right) \cos\left(\frac{\pi A_2^2}{2}\right) + \sin\left(\frac{30\pi}{180} + \pi\right) \sin\left(\frac{\pi A_2^2}{2}\right) \right]
 \end{aligned} \tag{19}$$

$$\begin{aligned}
 &\pi R_1 A_1 \left[\cos\left(\frac{3\pi}{180}\right) \sin\left(\frac{\pi A_1^2}{2}\right) + \sin\left(\frac{3\pi}{180}\right) \cos\left(\frac{\pi A_1^2}{2}\right) \right] \\
 &= \pi R_2 A_2 \left[-\cos\left(\frac{30\pi}{180} + \pi\right) \sin\left(\frac{\pi A_2^2}{2}\right) - \sin\left(\frac{30\pi}{180} + \pi\right) \cos\left(\frac{\pi A_2^2}{2}\right) \right]
 \end{aligned} \tag{20}$$

Similar to the method used in the 'standard-mirrored clothoid' category, these four equations, (17) to (20) were simultaneously solved to find the parameter values, yielding $A_1 = 0.5517$, $A_2 = 0.0661$, $R_1 = 3.9042$, and $R_2 = 32.5857$. An illustration of the graph for this category can be observed in Fig. 4a.

For the other two categories, 'both mirrored' and 'mirrored-standard', they were resolved using manipulations of Equations (9) to (12), resulting in the following values: $A_1 = 0.2428$, $A_2 = 0.5991$, $R_1 = 6.5529$, and $R_2 = 2.6556$ for 'both mirrored'. However, for 'mirrored-standard', no solution was produced by Mathematica's "FindRoot" algorithm, and the output from Mathematica stated, "The line search decreased the step size to within the tolerance specified by AccuracyGoal and PrecisionGoal but was unable to find a sufficient decrease in the merit function".

All parameter values for each category are presented in Table 1. Meanwhile, clear representations of the plotted graphs for each category are displayed in Fig. 4.

Parameter	Both Standard	Both Mirrored	Mirrored-Standard	Standard-Mirrored
A_1	0.5517	0.2428	n/a	0.5423
A_2	0.0661	0.5991	n/a	0.0768
R_1	3.9042	6.5529	n/a	3.9629
R_2	32.5857	2.9556	n/a	27.9815

Table 1: Parameter values for each category of double clothoid segments in the first case.

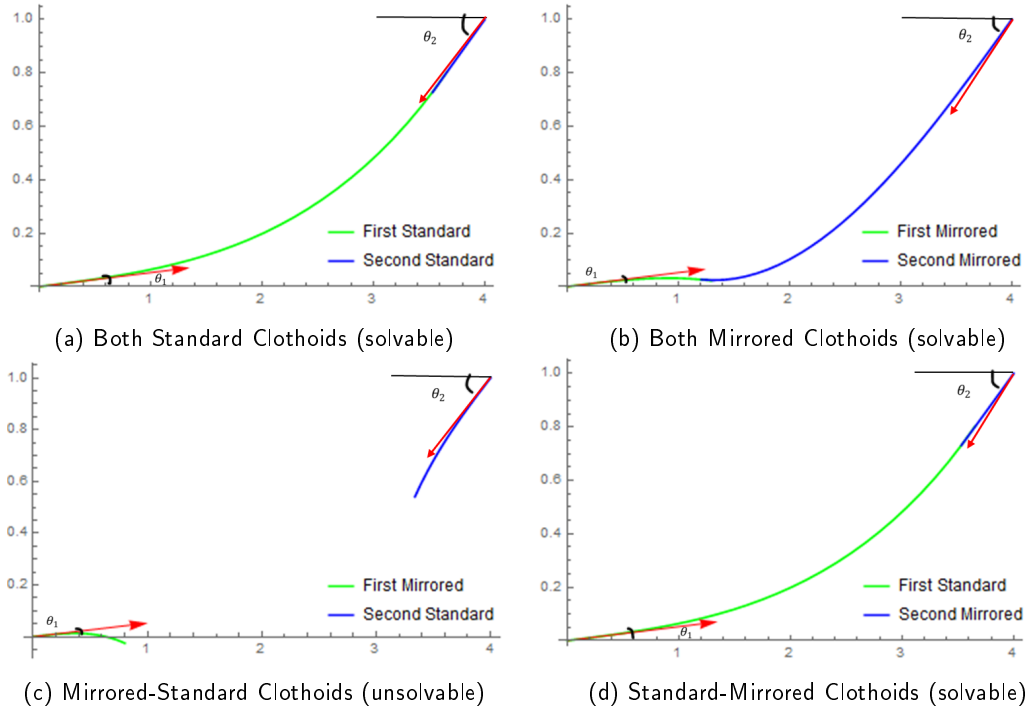


Figure 4: Illustration of four variations of double clothoid segments, showcasing specific examples of tangent angles, $\theta_1 = 3^\circ$ at the starting point and $\theta_2 = 30^\circ$ at the ending point.

In this first case, there are 3 categories that have solutions, namely 'Both Standard,' 'Both Mirrored,' and 'Standard-Mirrored.' To determine the most suitable category, we use the criterion of minimum curve length. Therefore, the formula used is from [25], which is

$$L_i = \frac{a_i^2}{R_i} \quad (21)$$

where L is the curve length, R is the radius, a is the scaling factor determined from the product of π , parameter A , and R , and i is the number of clothoid segment. Taking the calculation of curve length for the 'Both Standard' category as an example from Equation (21):

$$L_1 = \frac{a_1^2}{R_1} = \frac{(\pi A_1 R_1)^2}{R_1} = \frac{(\pi * 0.5517 * 3.9042)^2}{3.9042} = 11.7284 \quad (22)$$

$$L_2 = \frac{a_2^2}{R_2} = \frac{(\pi A_2 R_2)^2}{R_2} = \frac{(\pi * 0.0661 * 32.5857)^2}{32.5857} = 1.4052 \quad (23)$$

$$L_{total} = L_1 + L_2 = 13.1336 \quad (24)$$

From the calculations shown in Equations (22) to (24), it can be seen that the total curve length for the 'Both Standard' category is 13.1336. For the other categories, their values can be found in Table 2.

From Table 2, it is evident that the 'Standard-Mirrored' category yields the smallest curve length value. Therefore, the most appropriate choice for the first case is to use this category.

Length	Both Standard	Both Mirrored	Mirrored-Standard	Standard-Mirrored
L_1	11.7284	3.8127	n/a	11.5025
L_2	1.4052	10.4699	n/a	1.6289
L_{total}	13.1336	14.2826	n/a	13.1314

Table 2: Curve lengths for each category of double clothoid segments in the first case.

4.1.2 Case II: $\theta_1 = 30^\circ$, $\theta_2 = 5^\circ$

In the second case, we applied identical calculations as detailed in Section 4.1.1. The comprehensive outcomes of the parameter values are delineated in following Table 3. Furthermore, graphical depictions for each category are visually presented in Fig. 5. Interestingly, it became evident that for the 'standard-mirrored' category, no viable parameter values could be derived, signifying an absence of solutions for this particular category with the specified θ values. Nevertheless, all other categories yielded solutions.

Parameter	Both Standard	Both Mirrored	Mirrored-Standard	Standard-Mirrored
A_1	0.0232	0.5959	0.0243	n/a
A_2	0.5276	0.2779	0.5265	n/a
R_1	103.6230	2.5686	98.8332	n/a
R_2	4.5615	5.5056	4.5709	n/a

Table 3: Parameter values for each category of double clothoid segments in the second case.

Similar to the first case, there are 3 categories that have solutions, but this time they are 'Both Standard', 'Both Mirrored', and 'Mirrored-Standard'. Therefore, to determine the appropriate category choice, we use Equation (21). The curve length values for each category are shown in Table 4.

Length	Both Standard	Both Mirrored	Mirrored-Standard	Standard-Mirrored
L_1	0.5505	9.0021	0.5760	n/a
L_2	12.5319	4.1964	12.5054	n/a
L_{total}	13.0824	13.1985	13.0814	n/a

Table 4: Curve lengths for each category of double clothoid segments in the second case.

From the values shown in Table 4, it is evident that the 'Mirrored-Standard' category has the lowest value; therefore, this category is the most suitable choice.

4.1.3 Case III: $\theta_1 = 25^\circ$, $\theta_2 = 15^\circ$

For the third case, we continued to employ the same methodology as outlined in Section 4.1.1 previously. The respective parameter values for each category are tabulated in Table 5 for reference. In this instance, it is notable that only the 'both mirrored clothoid' category yielded solutions. Conversely, the other categories failed to produce any values for the involved parameters, indicating a lack of continuity between the two curvature segments for these categories, as depicted in Fig. 6.

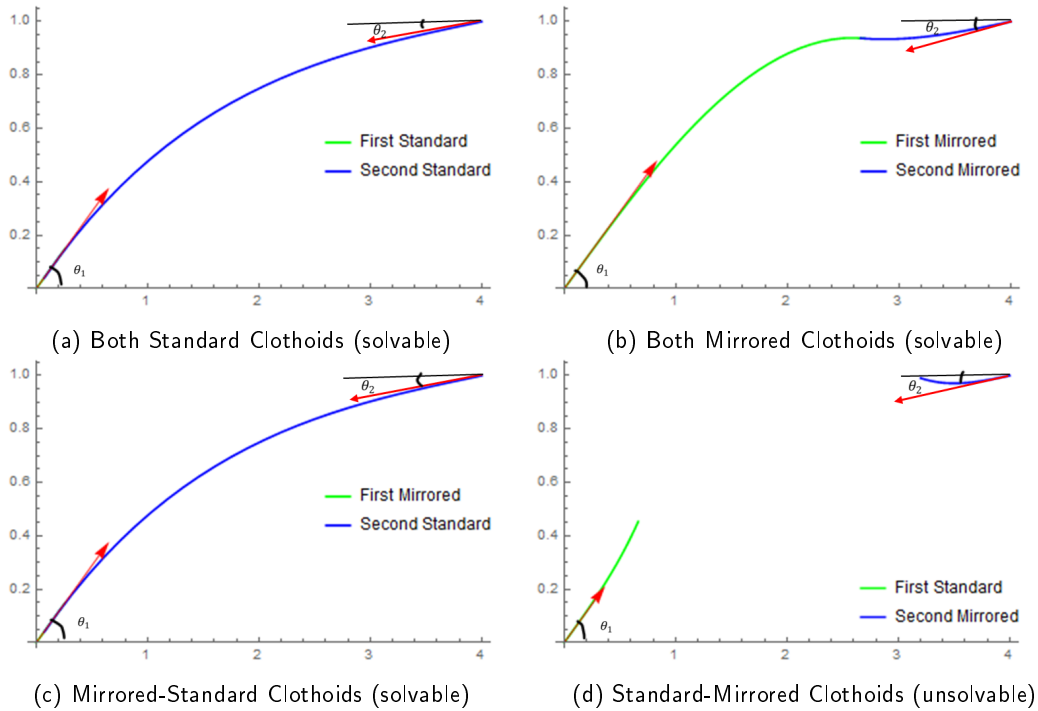


Figure 5: Illustration of four variations of double clothoid segments, showcasing specific examples of tangent angles, $\theta_1 = 30^\circ$ at the starting point and $\theta_2 = 5^\circ$ at the ending point.

Since only one category has a solution, there is no need to obtain curve length values for this case, and clearly, the 'both mirrored' category is the best choice.

Parameter	Both Standard	Both Mirrored	Mirrored-Standard	Standard-Mirrored
A_1	n/a	0.5187	n/a	n/a
A_2	n/a	0.3974	n/a	n/a
R_1	n/a	2.7822	n/a	n/a
R_2	n/a	3.6313	n/a	n/a

Table 5: Parameter values for each category of double clothoid segments in the third case.

From the three illustrated cases, it is evident that some cases yield solutions for more than one category, as observed in the first and second cases, contrasting with the third case, which offers only one category option. In this study, we employed the "FindRoot" algorithm in Mathematica to obtain solutions for each parameter. In instances where Mathematica failed to provide a solution, we note that the solution might still exist and need to be solved using different root finding approach. Future research endeavors may delve deeper into this matter.

Based on this study, decisions need to be made regarding the selection of category types when multiple solutions are available. The choice depends on selecting the solution with the minimum arc length using the previously stated formula.

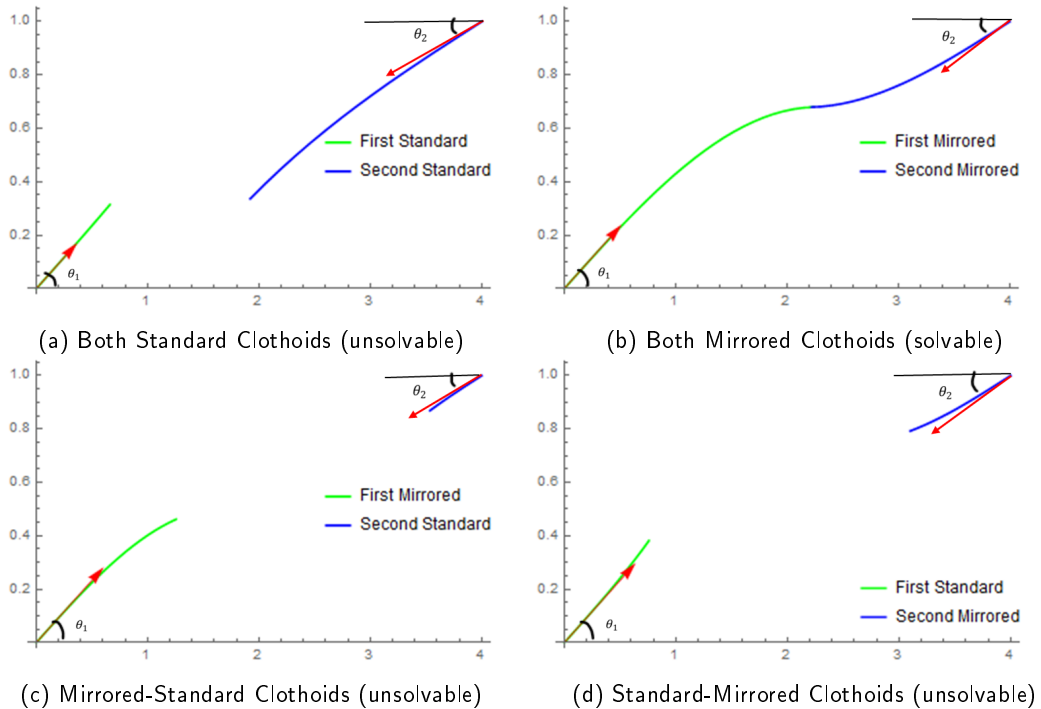


Figure 6: Illustration of four variations of double clothoid segments, showcasing specific examples of tangent angles, $\theta_1 = 25^\circ$ at the starting point and $\theta_2 = 15^\circ$ at the ending point.

4.2 Multiple Clothoid Segments Going Through a Predetermined Intermediate Point

In this study, we also demonstrate that the curvature of these double clothoid segments can pass through predetermined points along with the tangent direction at the specified initial and final points. The result of using this method is that multiple clothoid segments will be employed. To illustrate the discussion of this situation, we use the example of initial and final points as $(0,0)$ and $(4,1)$. The tangent direction at the starting point is 20° , representing θ_1 , and at the end point, it is 30° , representing θ_3 . Meanwhile, the predetermined intermediate point traversed by the curve is $(2.2,0.6)$ with a tangent direction passing through it at 15° , noted by θ_2 . Fig. 7 illustrates this scenario: Fig. 7a displays the specific labeling of multiple clothoid segments passing through a predetermined intermediate point, along with their tangent angles. In contrast, Fig. 7b shows the same trajectory without the specific labeling. This demonstrates the method's capability to handle such situations effectively.

4.3 Simulated Result of Differential Drive Robot

For the sake of discussion, we conducted several simulations on the movement of the Pioneer 3DX robot using the CoppeliaSim simulator platform for each category of double clothoid segments. Here, we assess whether the robot can follow the path generated from these double clothoid segments. Minor errors or discrepancies may arise due to various factors, as stated in [27]. However, overall, the robot's movement remains within the intended trajectory and final target point.

The first simulation, showcased in Fig. 8, derives from the outcomes depicted in Fig. 4d on Case I, specifically focusing on the 'standard-mirrored clothoid' category. The robot's movement trajectory closely to

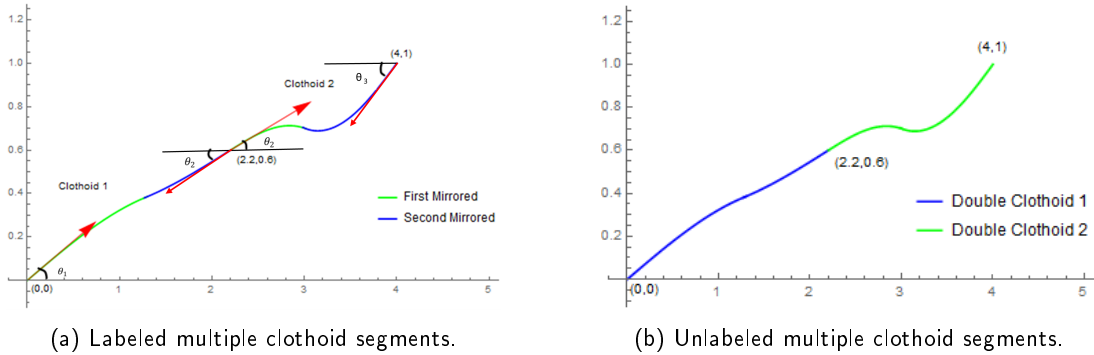


Figure 7: Illustration of multiple clothoid segments passing through a predetermined intermediate point.

the planned path as indicated by clothoid 1 and 2 from the graph.

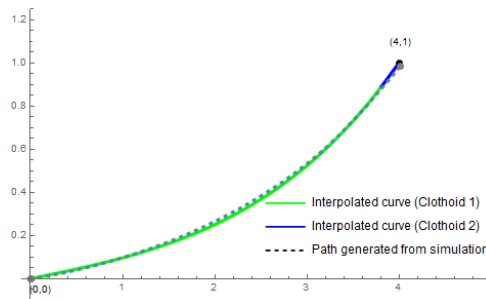


Figure 8: Visualization of robot simulation on 'standard-mirrored' clothoids from Case I, as depicted in Fig. 4d.

Subsequent simulations delve into the 'both standard' category, as visually represented in Fig. 9, with data extracted from Fig. 5a. Likewise, the robot's trajectory depicted in the generated path closely aligns with the intended movement represented by clothoids 1 and 2 in this graph. Similarly, the robot movement shown in generated path is close to our planned movement shown by clothoid 1 and 2 of this graph.

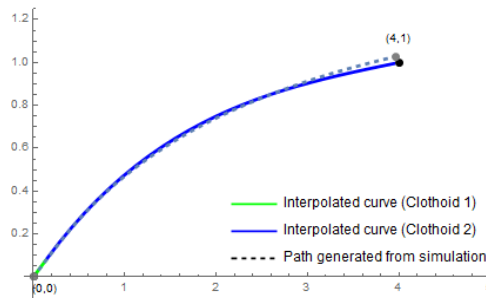


Figure 9: Visualization of robot simulation on 'both standard' clothoids from Case II, as depicted in Fig. 5a.

Further analyses were conducted based on the results depicted in Fig. 5c, representing the 'mirrored-

standard' category, as illustrated in Fig. 10. Likewise, the robot's trajectory depicted in the generated path closely aligns with the intended movement represented by clothoid 1 and 2 in this graph.

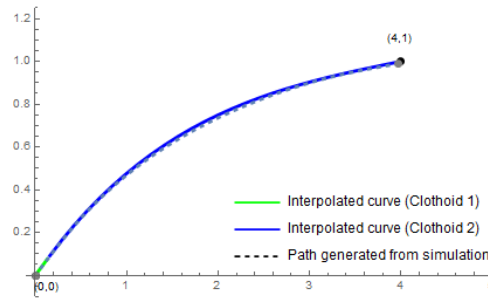


Figure 10: Visualization of robot simulation on 'mirrored-standard' clothoids from Case II, as depicted in Fig. 5c.

Lastly, the simulation is performed using data obtained from Fig. 6b, focusing on the 'both mirrored' category where the robot requires to make a turn the right before turning to the left as illustrated in Fig. 11. Even if the robot has to turn, then the simulated path is still close. However, there is a slight error at the ending point.

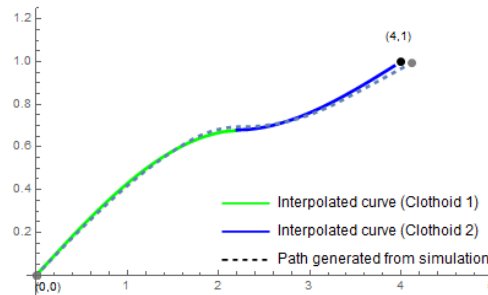


Figure 11: Visualization of robot simulation on 'both mirrored' clothoids from Case III, as depicted in Fig. 6b.

From the four simulations conducted, it is evident that the robot's path closely resembles the path generated by double clothoid segments. This highlights the capability of clothoids in producing smoother paths, allowing for more flexible adjustments in the tangent angles at the start and end of the trajectory. In this study, we primarily focused on a graphical analysis of how the robot's path aligns with the trajectory generated by double clothoids. For future investigations, a detailed examination of the error values between these two paths using suitable algorithms could provide valuable insights.

Moreover, during the simulations, ensuring optimal computer performance is crucial. We acknowledge that each category requires multiple simulations until highly optimal results are obtained. Considerations include running no other applications on the computer during the simulations, ensuring that only the CoppeliaSim Simulator and Matlab software are active during the process. Failure to account for this factor may lead to disruptions in the results. Similarly, in real life robot, the optimum movement can be planned if the robot has an optimum physical capacity including sufficient battery levels, efficient hardware energy consumption, and energy-efficient locomotion [29].

4.4 Comparison with Previous Study

The preceding study conducted by [27] addressed scenarios where point interpolation depended on a single circular arc. In such cases, determining the tangent angle at the initial point posed no significant challenge. However, computing the tangent at the target point required subsequent computation. This intricate process entailed integrating the parameter A into the differentiation of $C_s(t, \theta, 1)$, expressed as $C'_s(A, \theta_1, 1) = (p, q)$, followed by $\tan^{-1}(\frac{q}{p})$ to ascertain the tangent angle. Notably, in this instance, θ_1 is set to 0^0 , while θ_2 is assigned 42^0 . The interpolated path alongside the simulated path is illustrated in Fig. 12a, effectively showcasing the outcomes of the analysis.

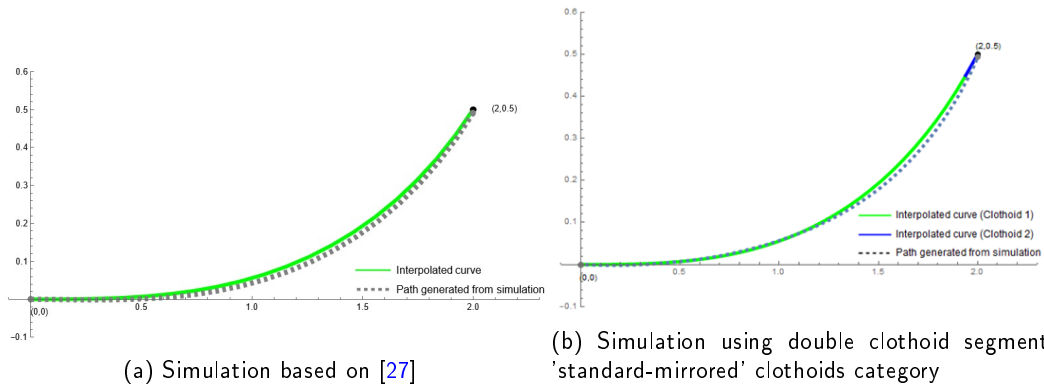


Figure 12: Comparison of curve interpolation with simulated paths.

The integration of double clothoid segments gives an extra advantage as we are able to define start and end tangent angle. To validate our approach, we compare our findings with results from previous studies, as depicted in Fig. 12b, showing remarkable consistency despite employing different techniques.

Furthermore, other techniques, such as using G^2 log-aesthetic splines [17], could be explored in future research. However, our demonstration indicates that the double clothoid approach effectively guides the robot along the specified trajectory smoothly.

Additionally, we explore a scenario where distinct tangent angles are assigned to each point, providing further evidence of our method's efficacy and adaptability. This discussion demonstrates the robustness of our approach in addressing various trajectory planning challenges, highlighting its potential to enhance motion planning for differential drive mobile robots.

5 CONCLUSION

We present our inventive strategy in clothoids through the incorporation of double clothoid segments, simplifying the calculation process despite the inherent complexity of clothoid formulations. This approach enhances trajectory planning by facilitating the determination of tangent directions for both the initial and final points of robot movement. This simplicity proves invaluable in navigating the intricate terrain of robotics, empowering robots to overcome even the most formidable challenges effortlessly.

A detailed explanation of the construction of double clothoid segments resulting in four categories - 'both standard,' 'both mirrored,' 'mirrored-standard,' and 'standard-mirrored' - was provided. The formulation of these segments is discussed and can be easily derived. One notable accomplishment of this study is the ability to predefine the tangent angles for the start and end points of the trajectory, providing greater flexibility and discuss in the context of differential drive robot.

In situations where multiple category options exist for a given initial and final tangent value, we are free to choose any category. However, for future research, we will explore the most optimal category selection using appropriate algorithms. Simulations were conducted on the Pioneer 3-DX differential drive robot to assess the extent to which the robot's movement can follow the trajectories generated by these double clothoid segments. This study also includes a comparison with previous research in [27], demonstrating that our approach can achieve similar results with slight improvements, particularly with the predefined start and end tangent angles.

This study is expected to serve as a steppingstone towards the development of more advanced trajectory generation methods, aiding researchers in enhancing their focus on motion planning studies.

Mohd Fazril Izhar Mohd Idris, <https://orcid.org/0009-0008-5231-3785>

Ahmad Ramli, <https://orcid.org/0000-0003-0853-3920>

Wan Zafira Ezza Wan Zakaria, <https://orcid.org/0000-0002-6421-840X>

REFERENCES

- [1] Webots documentation adept's pioneer 3-dx. <https://www.cyberbotics.com/doc/guide/pioneer-3dx?version=R2021a>.
- [2] Arshad, S.; Sualeh, M.; Kim, D.; Nam, D.V.; Kim, G.W.: Clothoid: an integrated hierarchical framework for autonomous driving in a dynamic urban environment. *Sensors*, 20(18), 5053, 2020. <http://doi.org/10.3390/s20185053>.
- [3] Bertolazzi, E.; Frego, C.; Frego, M.; Hosseini, S.M.; Peer, A.: The clothoid: a historical, literary and artistic introduction with applications to technology. In 2023 8th IEEE History of Electrotechnology Conference (HISTELCON), 16–19. IEEE, 2023. <http://doi.org/10.1109/HISTELCON56357.2023.10365736>.
- [4] Bertolazzi, E.; Frego, M.: On the G^2 hermite interpolation problem with clothoids. *Journal of Computational and Applied Mathematics*, 341, 99–116, 2018. <http://doi.org/10.1016/j.cam.2018.03.029>.
- [5] Chen, Y.: Clothoid spline based path planning. Ph.D. thesis, Nanyang Technological University, 2017.
- [6] Chi, P.; Wang, Z.; Liao, H.; Li, T.; Tian, J.; Wu, X.; Zhang, Q.: Am-rrt*: An automatic robot motion planning algorithm based on rrt. In *International Conference on Neural Information Processing*, 91–103. Springer, 2023. http://doi.org/10.1007/978-981-99-8079-6_8.
- [7] Connor, D.; Krivodonova, L.: Interpolation of two-dimensional curves with euler spirals. *Journal of computational and applied mathematics*, 261, 320–332, 2014. <http://doi.org/10.1016/j.cam.2013.11.009>.
- [8] Ishikawa, H.; Noguchi, K.; Maki, R.; Naitoh, H.: Path generation with clothoid curve using image processing for two-wheel-drive autonomous mobile robots. *IFAC Proceedings Volumes*, 42(16), 523–528, 2009. <http://doi.org/10.3182/20090909-4-JP-2010.00089>.
- [9] Javid, M.; Haleem, A.; Singh, R.P.; Suman, R.: Substantial capabilities of robotics in enhancing industry 4.0 implementation. *Cognitive Robotics*, 1, 58–75, 2021. <http://doi.org/10.1016/j.cogr.2021.06.001>.
- [10] Kurenkov, M.; Potapov, A.; Savinykh, A.; Yudin, E.; Kruzhev, E.; Karpyshev, P.; Tsetserukou, D.: Nfomp: Neural field for optimal motion planner of differential drive robots with nonholonomic constraints. *IEEE Robotics and Automation Letters*, 7(4), 10991–10998, 2022. <http://doi.org/10.1109/LRA.2022.3196886>.
- [11] Lambert, E.; Romano, R.; Watling, D.: Optimal path planning with clothoid curves for passenger comfort. In *Proceedings of the 5th International Conference on Vehicle Technology and Intelligent Transport Systems (VEHITS 2019)*, vol. 1, 609–615. SciTePress, 2019. <http://doi.org/10.5220/0007801806090615>.

- [12] Lambert, E.D.; Romano, R.; Watling, D.: Optimal smooth paths based on clothoids for car-like vehicles in the presence of obstacles. *International Journal of Control, Automation and Systems*, 19, 2163–2182, 2021. <http://doi.org/10.1007/s12555-020-0179-1>.
- [13] Lin, P.; Javanmardi, E.; Tsukada, M.: Clothoid curve-based emergency-stopping path planning with adaptive potential field for autonomous vehicles. *IEEE Transactions on Vehicular Technology*, 2024.
- [14] Loganathan, A.; Ahmad, N.S.: A systematic review on recent advances in autonomous mobile robot navigation. *Engineering Science and Technology, an International Journal*, 40, 101343, 2023. <http://doi.org/10.1016/j.jestch.2023.101343>.
- [15] Meek, D.S.; Walton, D.J.: Offset curves of clothoidal splines. *Computer-Aided Design*, 22(4), 199–201, 1990. [http://doi.org/10.1016/0010-4485\(90\)90048-H](http://doi.org/10.1016/0010-4485(90)90048-H).
- [16] Meek, D.S.; Walton, D.J.: An arc spline approximation to a clothoid. *Journal of Computational and Applied Mathematics*, 170(1), 59–77, 2004. <http://doi.org/10.1016/j.cam.2003.12.038>.
- [17] Miura, K.T.; Shibuya, D.; Gobithaasan, R.U.; Usuki, S.: Designing log-aesthetic splines with G^2 continuity. *Computer-Aided Design and Applications*, 10(6), 1021–1032, 2013. <http://doi.org/10.3722/cadaps.2013.1021-1032>.
- [18] Othman, N.; Reif, U.; Ramli, A.; Misro, M.: Manoeuvring speed estimation of a lane-change system using geometric hermite interpolation. *Ain Shams Engineering Journal*, 12(4), 4015–4021, 2021. <http://doi.org/10.1016/j.asej.2021.02.027>.
- [19] Panwar, V.S.; Pandey, A.; Hasan, M.E.: Generalised regression neural network (grnn) architecture-based motion planning and control of an e-puck robot in v-rep software platform. *acta mechanica et automatica*, 15(4), 209–214, 2021. <http://doi.org/10.2478/ama-2021-0027>.
- [20] Rubio, F.; Valero, F.; Llopis-Albert, C.: A review of mobile robots: Concepts, methods, theoretical framework, and applications. *International Journal of Advanced Robotic Systems*, 16(2), 1729881419839596, 2019. <http://doi.org/10.1177/1729881419839596>.
- [21] Sani, M.; Hably, A.; Robu, B.; Dumon, J.; Meslem, N.: Real-time dynamic obstacle avoidance for a non-holonomic mobile robot. In *2023 IEEE 32nd International Symposium on Industrial Electronics (ISIE)*, 1–6. IEEE, 2023. <http://doi.org/10.1109/ISIE51358.2023.10227920>.
- [22] Smith, J.: Rise of the machines: Emerging trends in robotics. *International Journal of Research and Review Techniques*, 2(3), 1–8, 2023.
- [23] Štefek, A.; Pham, V.T.; Krivanek, V.; Pham, K.L.: Optimization of fuzzy logic controller used for a differential drive wheeled mobile robot. *Applied Sciences*, 11(13), 6023, 2021. <http://doi.org/10.3390/app11136023>.
- [24] Thai, N.H.; Ly, T.T.K.; Thien, H.; Dzung, L.Q.: Trajectory tracking control for differential-drive mobile robot by a variable parameter pid controller. *International Journal of Mechanical Engineering and Robotics Research*, 11(8), 614–621, 2022. <http://doi.org/10.18178/ijmerr.11.8.614-621>.
- [25] Vázquez-Méndez, M.E.; Casal, G.: The clothoid computation: A simple and efficient numerical algorithm. *Journal of Surveying Engineering*, 142(3), 04016005, 2016. [http://doi.org/10.1061/\(ASCE\)SU.1943-5428.0000177](http://doi.org/10.1061/(ASCE)SU.1943-5428.0000177).
- [26] Walton, D.J.; Meek, D.S.: A controlled clothoid spline. *Computers & Graphics*, 29(3), 353–363, 2005. <http://doi.org/10.1016/j.cag.2005.03.008>.
- [27] Wan Zakaria, W.Z.E.; Ramli, A.; Misro, M.Y.; Ab Wahab, M.N.: Motion planning of differential drive mobile robot using circular arc. *Engineering Letters*, 32(1), 2024.
- [28] Wilde, D.K.: Computing clothoid-arc segments for trajectory generation. *Intelligent Robots and Systems*, 2440–2445, 2009. <http://doi.org/10.1109/IROS.2009.5354700>.

- [29] Wu, M.; Yeong, C.F.; Su, E.L.M.; Holderbaum, W.; Yang, C.: A review on energy efficiency in autonomous mobile robots. *Robotic Intelligence and Automation*, 43(6), 648–668, 2023. <http://doi.org/10.1108/RIA-05-2023-0060>.
- [30] Yang, Y.; Pan, J.; Wan, W.: Survey of optimal motion planning. *IET Cyber-systems and Robotics*, 1(1), 13–19, 2019. <http://doi.org/10.1049/iet-csr.2018.0003>.
- [31] Yoshida, N.; Saito, T.: Interactive aesthetic curve segments. *The Visual Computer*, 22, 896–905, 2006. <http://doi.org/10.1007/s00371-006-0076-5>.
- [32] Zhou, C.; Huang, B.; Fränti, P.: A review of motion planning algorithms for intelligent robots. *Journal of Intelligent Manufacturing*, 33(2), 387–424, 2022. <http://doi.org/10.1007/s10845-021-01867-z>.